2025
12(1), 1151

Biomedical and
Therapeutics LETTERS

Exploring the therapeutic potential of Esculin in the treatment of bladder cancer

Yenumala Vamshidhar Reddy

Department of Pharmacy, Osmania University, Hyderabad. India.

Submitted on: 17-Nov-2024, Accepted and Published on: 07-Jan-2025

Article

ABSTRACT

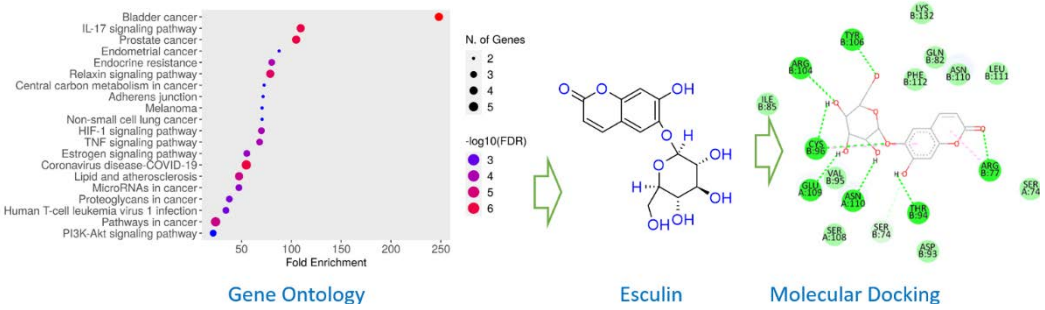

This research highlights the potential of Esculin as a promising treatment for bladder cancer, supported by insilico molecular docking and network pharmacology analyses. The study identified key targets, including GAPDH, TNF, MMP9, EGFR, and IL2, which play crucial roles in pathways associated with bladder cancer, such as IL-17 and TNF signalling. Esculin showed a strong binding affinity to these targets, especially to TNF, indicating its therapeutic potential. Calculations of binding free energy using the Molecular Mechanics Poisson-Boltzmann Surface Area (MMPBSA) method revealed the interaction dynamics, with the TNF-Esculin complex having a favourable binding free energy of -8.92 kcal/mol. This was primarily influenced by van der Waals forces (-16.1 kcal/mol) and electrostatic interactions (-3.57 kcal/mol), along with significant solvation effects. Energy decomposition analysis identified specific residues in the binding pocket that contribute to the stability of the complex, reinforcing Esculin's prospects for drug development. Moreover, principal component analysis (PCA) of the molecular dynamics (MD) simulations illustrated the dynamic behaviour of the TNF-Esculin complex, indicating a high level of stability, as evidenced by its smaller spatial occupation in trajectory plots. Overall, these findings strongly advocate for further exploration of Esculin as a novel therapeutic agent for bladder cancer, highlighting the need for additional experimental validation and drug development initiatives.

Keywords: Esculin, Bladder Cancer, Network Pharmacology, Molecular Docking, Molecular Dynamic Simulation

INTRODUCTION

Bladder cancer, otherwise referred to as urological cancer or urinary bladder cancer, is ranked 10th in the world. It has been rising steadily in the world, especially in the developed nations.[1] It is a hollow organ located in the lower abdomen, whose major function is to store urine it receives from the kidneys via the ureter until micturition. Specialised transitional epithelial cells that line the urinary bladder and the urinary tract called urothelial cells, adjust to the amount of produced urine by flattening under pressure. The lining of the bladder is smooth muscle, a part that relaxes to accommodate greater volumes and also contracts - under voluntary or reflex control - to expel urine down the urethra and out of the body.[2] Urothelial cells lining the bladder and urinary tract are continually exposed to environmental, probably mutagenic, agents filtered into the urine by the kidneys. Not surprisingly, 90% of bladder cancer consists of such urothelial cells, mainly localized in the bladder but happening rarely in the urinary tract as well, especially in developed countries. Whereas prognosis in localized forms of urothelial cancer is excellent, once the smooth muscle is invaded, survival rates are very poor.[3] Probably the most common risk factor for bladder cancer is smoking, which accounts for about two-thirds of all cases in men and one-third in women. Smokers have about a fourfold increased risk compared to non-smokers.[4] Because the bladder's function is to store urine, there is ample time for carcinogens in the urine to affect the bladder. The contacting substances remain in constant contact within the genitourinary system until eliminated, thus the high rate for urothelial cancers.[5,6]

Esculin or Aesculin, is a natural compound present in various plants, particularly in tree bark for example, that of the horse chestnut (*Aesculus hippocastanum*) but also in herbs like the bearberry plant. This phytochemical is classified within the large group of compounds called glycosides, characterized by being susceptible to hydrolysis that is, they split into a sugar and another compound upon reacting with the corresponding enzyme or under particular conditions.[7] The chemical composition of esculin includes a glucose molecule bound to a coumarin nucleus. This peculiar molecular arrangement has vested a few interesting

*Corresponding Author: Yenumala Vamshidhar Reddy
Email: Vamshiv890@gmail.com:

URN:NBN:sciencein.btl.2025.v12.1151
DOI: 10.62110/sciencein.btl.2025.v12.1151

https://pubs.thesciencein.org/btl

properties and biological activities, which became one of the research interests, though it exerts an important variety of pharmacological activities. Anti-inflammatory, antioxidant, and antimicrobial effects have been highlighted as the first two provoking research toward potential therapeutics in the treatment of inflammatory disorders, oxidative stress-related conditions, and infectious diseases, respectively. Endocrine, Pharmacological, and Neuroprotective Activity.[8] Apart from the pharmacological aspects, it has also been studied in the context of plant defence and as a phytochemical marker with taxonomic significance. That means that, apart from the medicinal uses, it exerts an ecological role as a potential deterrent against herbivores and pathogens in some plant species.[9] The pharmacological profile of esculin indicates its high potential for various medicinal applications. According to research, it is a drug with powerful antioxidant effects and can act as a free radical scavenger, protecting the cells from oxidative stress.[10] It also exhibits anti-inflammatory properties that have been investigated for its potency to reduce inflammation and associated disorders. On the other hand, it has shown antimicrobial activity against a broad range of bacterial and fungal pathogens, making it a potential candidate for developing novel antimicrobial agents.[11]

A major principle of treating diseases is to find therapeutics that can act on multiple proteins involved in the characteristics of a given disease. One such helpful method is to construct multiple networks with which to understand the gene targets, illnesses, medications involved, and the related Kyoto Encyclopaedia of Genes and Genomes pathways, thereby involving systems biology and computational biology within network pharmacology.[12,13,14] Moreover, the energies of binding between ligands and receptors are computable through molecular docking and hence help predict the right binding modes.[15]

This work aims at exploring the possible targets and mechanisms of action for Esculin to treat bladder cancer using the methods of network pharmacology and molecular docking. It is to provide new therapeutic targets for bladder cancer and provide a molecular basis for the application of Esculin in treating such diseases.

MATERIALS AND METHODS

2.1 Obtaining Esculin-Related Target Genes

The canonical chemical structure and SMILES file of Esculin are obtained from PubChem Database (https://pubchem.ncbi.nlm.nih.gov/) [16]. Subsequently, Esculin target genes were obtained with the help of the SwissTargetPrediction (http://www.swisstargetprediction.ch/) and STITCH (http://stitch.embl.de/) databases respectively [17,18]. The targets for esculin chosen were combined, removing duplicates for the determination of target genes.

2.2 Obtaining Bladder Cancer-Related Target Genes

Using the keyword "Bladder Cancer," the Bladder Cancer-associated target genes from the GeneCards database were chosen (https://www.genecards.org/) [19]. The highest score value obtained is 52.01 while the lowest is 0.19. The potential target for bladder cancer is supposed to have a score of not less than five in order to identify the target with a score of about 6.2. The chosen targets were combined and the duplicate data eliminated from the investigation in order to determine the target genes for bladder cancer.

Obtaining Potential Common Targets

Using the online tool Venny 2.1, import the common targets in a Venn diagram to find overlapping potential targets of Esculin and Bladder Cancer (https://bioinfogp.cnb.csic.es/tools/venny/).

Protein-Protein Interaction (PPI) Network Construction and Detection of Hub Targets

Using the search tool for retrieval of interacting genes/proteins, an interaction network was constructed with version 12.0 of STRING to identify an interaction network of the target genes of Esculin (https://string-db.org/) and the PPI network was generated with a minimum required interaction score of >0.4 [20]. Hub genes were identified from the data collected that was imported into Cytoscape v.3.10.2, based on the degree method and higher-degree nodes using the CytoHubba plugin.[21,22,23]

Pathways and Gene Ontology(GO) Enrichment Analysis

Currently, one of the prevalent ways of investigating available genomic data, particularly huge-scale transcriptome data, is Gene Ontology analysis. Three groups examined potential targets for GO functional enrichment: biological process, cellular component, and molecular function.[24,25] Pathways of the hub genes and diseases were investigated via the DAVID database (https://david.ncifcrf.gov/tools.jsp) and Shiny GO software version 0.76, (http://bioinformatics.sdstate.edu/go76/) in the Kyoto Encyclopedia of Genes and Genomes (https://www.genome.jp/kegg/) respectively.[26,27] Gene set enrichment results with $p < 0.05$ were considered statistically significant.

Molecular Docking

The three-dimensional structures of Esculin were made with the Auto dock vina software. The generated esculin was ionized with the OPLS4 force field to produce tautomeric states after which they were converted into their three-dimensional (3D) structures.[28,29] The 3D crystal structures of the target proteins were selected and retrieved from the Protein Data Bank (PDB) (https://www.rcsb.org/). Protein production provided incorporation of hydrogen where none was available, closing the gaps of loops and modifying protonation states of side chains after stripping water molecules from the crystal structures. Hydrogens, charges, and bond order were assigned to heavy atoms. Selenomethionines were converted into methionines after removing all water molecules. The selected protein was first broken down and preparation was then done for the purpose of creating the grid.[30] A docking score was generated upon calculating the final scoring using the energy-minimized poses. The best-docked site for each ligand was determined by choosing the site with the lowest possible Docking score value.

ADMET Analysis

In the ADMET analysis of Esculin, predictions from SwissADME indicate good oral bioavailability and moderate distribution, with limited potential for crossing the blood-brain barrier.[31] Metabolism insights from ProTox III suggest involvement of key cytochrome P450 enzymes, while renal

excretion is likely a primary elimination route [32]. Toxicity assessments show a low to moderate toxicity profile, indicating a favorable safety margin for therapeutic use. Overall, these in silico analyses suggest that esculin possesses promising pharmacokinetic properties warranting further experimental validation.

Molecular Dynamics Simulation

The molecular dynamics simulations have been done on a workstation running under an AMD Ryzen 5 7600X Processor, 32 GB RAM with an NVIDIA GeForce RTX 3060 12GB as the GPU. The platform used in this study for investigating the thermodynamic stability of the Protein-Ligand complex was GROMACS 2024.2 version.[33] The latest CHARMM all-atom force field was employed in performing MD simulations [34]. Topology files, separate for receptor and for ligand, were prepared with the help of different external tools like Swiss Param before simulation [35]. With the optimized structure, we generated a topology for the ligand using the CHARMM General Force Field program: CGenFF.[36] In the CHARMM all-atom force field itself, all H atoms of the ligand are explicitly represented. We applied a well-known water model: TIP3P-Transferable Intermolecular Potential with 3 Points for simulation in water. In the course of solvation, the bare protein and protein-ligand complex were solvated in the triclinic box having specific boundary conditions. As per the procedure, Na^+ & Cl^- ions were added for electrically neutralizing the system. Before simulation, we performed energy minimization on the system to sort out any bad starting structures and to minimize solute structure in vacuum before introducing solvent molecules. The steepest descent algorithm[37] has been used for energy minimization of the system with varying time of ps/ns for 5,00,000 steps. The applied algorithm has a cut-off up to 1000 kJmol−1 for reducing the steric clashes. The MD simulation has been started with the minimization of the system. The minimization has been achieved at two phases each having 500,000 steps. In first part, equilibration was obtained having each step of 2 fs with a boundary condition of constant number of particles, volume and temperature. We used 10,000 ps NVT equilibration. In the second phase, the equilibration achieved under 1 atmosphere pressure at 300 K. Here the boundary condition kept as constant NPT. For the computation of the equilibration step, LINCS algorithm was applied for covalent bond constraints [38]. Evaluating the non-bonded interaction energy between two species would be a useful way to quantify the interaction strength between a ligand and a protein, rather than calculating the free energy of the system. In the case of non-bonded energy calculation, we have used short-range Lennard-Jones and Coulomb interaction energies [39]. All calculations have used a 1.2 nm radius cut-off. Long-range electrostatics has been calculated using the PME method [40] with a Fourier grid spacing of 0.16 nm. The temperature inside the box has been kept by applying the Berendsen temperature coupling method, otherwise known as V-rescale. In addition to this, to obtain NPT equilibration, Parrinello-Rahman pressure coupling and C-rescale have been used. The time parameter has been fixed at 50,000 ps, being 0.002 fs for each step in the last stage of simulation. The MD simulation data and output for energy minimization have been used to visualize the following thermodynamic parameters: potential energy, kinetic energy, total energy, temperature, RMSD, RMSF, SASA, etc., of the Receptor-Ligand complex. After running the final step of each simulation, trajectories were obtained. Then, obtained trajectories and results were analysed by using the graphical tool xmgrace. Least-square fitting method was used for evaluating RMSD for Protein backbone and Ligand. Similarly, RMSF was obtained for protein backbone. In order to compute the total SASA, the tool sasa has been used. SASA is a measure of the receptor area exposed to the solvents during the simulation process. The number of hydrogen bonds and distribution of intermolecular hydrogen bond lengths have been calculated.

2.9 Binding Free Energy Calculations (MM/PBSA)

The systems chosen for further investigation underwent Molecular Mechanics/Poisson-Boltzmann Surface Area (MM/PBSA) computations using the GROMACS software suite's g_mmpbsa tool [41]. The MM/PBSA method was used to determine the binding free energy of the MD simulation trajectories.

$$\Delta G_{binding} = \Delta G_{complex} - (\Delta G_{protein} + \Delta G_{ligand})$$

where:

$\Delta G_{binding}$ = Binding Free Energy.

$\Delta G_{complex}$ = Solvation free energy of the complex.

$\Delta G_{protein}$ = Solvation free energy of the free protein.

ΔG_{ligand} = Solvation free energy of the free ligand.

Generally, free energy of solvation is often computed making use of the Poisson-Boltzmann (PB) or Generalized Born (GB) models. It describes the free energy related to the interaction between the solvent and the biomolecule. With the notation used here, the superscript symbol denotes the change in the energy due to solvation of the solute that follows.

2.10 Principal Component Analysis (PCA)

Principal component analysis (PCA) has been used in exploring the essential dynamics of protein-ligand complexes. This is a multivariate statistical technique that reduces data linearly, starting from a given input in form of a covariance matrix to obtain the most prominent features or simply the dominant motion in complex trajectories [42]. The gmx_covar module available in the GROMACS packages was used to create and analyse a Cartesian coordinate covariance matrix for calculating the eigenvectors and eigenvalues. Using the gmx_anaeig module of GROMACS, each plot for the eigenvectors of the protein-ligand complex MD trajectories was examined.

RESULTS AND DISCUSSION

3.1 Screening of Potential Bladder Cancer Targets for Esculin

The tool identified the potential targets for Esculin and Bladder Cancer from several databases. Database searching and analyzing on the SwissTargetPrediction gave 100 possible targets associated with Esculin. Integration of the values and removal of

duplication to identify the putative targets associated with Esculin yielded a total. Meanwhile, database querying and analysis of GeneCards returned 3500 potential targets associated with bladder cancer, while 595 prospective targets were recovered after integration with the duplicate values removed and having a score of at least 5. Venn diagram analysis was used to probe for overlapping targets in the identified potential targets of bladder cancer and Esculin. of all targets, 23 shared targets (3.4% of the total) were found. In our analysis of the target overlap between Esculin and Bladder Cancer, we found significant commonalities as depicted in Figure 1.

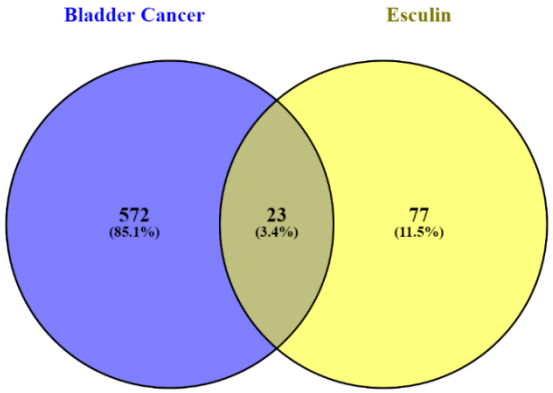

Figure 1. Venn diagram of common targets between Esculin and Bladder Cancer: Targets related to Bladder Cancer and Esculin are represented in blue and yellow, respectively, in the circle. Their intersection is the common target of Bladder Cancer and Esculin.

3.2 PPI Network Construction and Hub Targets Analysis

These 23 common targets were mapped into the STRING v12.0 database to build a PPI network, which was used to describe the interactions of these potential targets. The results are as follows: 107 edges with 23 nodes in a PPI network, a clustering coefficient of 0.806, and an average node degree of 9.3. In this case, the PPI enrichment p-value resulted in less than 1.0 × 10−16, while the expected number of edges was 40; this value is much below the one obtained by real edges. A network diagram of the hub targets of Bladder Cancer and Esculin was drawn after analysis in the PPI network using the cytoHubba add-on of Cytoscape software to determine the top 10 according to the degree method as the hub target of the PPI network. Results indicated that the top 10 hub targets were Glyceraldehyde-3-Phosphate Dehydrogenase (GAPDH), Tumor Necrosis Factor (TNF), Matrix Metallopeptidase 9 (MMP9), Epidermal Growth Factor Receptor (EGFR), Interleukin 2 (IL2), Matrix Metallopeptidase 3 (MMP3), Matrix Metallopeptidase 1 (MMP1), Matrix Metallopeptidase 7 (MMP7), Matrix Metallopeptidase 12 (MMP12), and Mitogen Activated Protein Kinase 1 (MAPK1). The PPI network analysis, shown in Figure 2, illustrates the interactions among the common targets between Bladder Cancer and Esculin. Figure 3 illustrates the top 10 hub targets within the PPI network, as determined by the Degree method in cytoHubba. Figure 4 illustrates the top 10 hub genes as determined by the Degree method, with a bar chart displaying their respective connectivity scores.

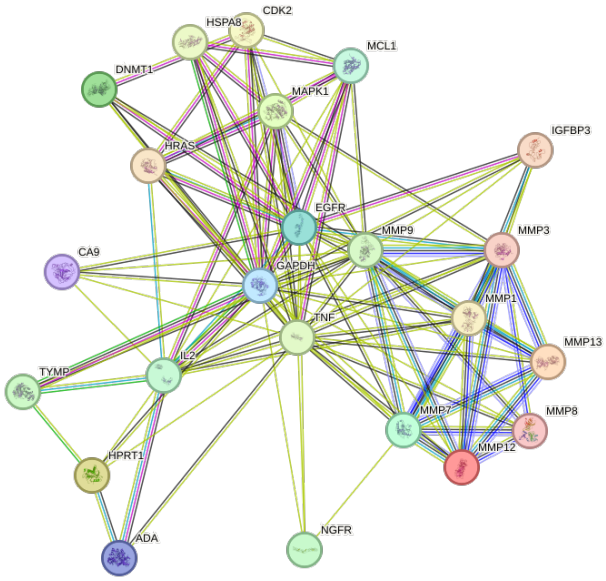

Figure 2. PPI Network of Common targets between Bladder Cancer and Esculin.

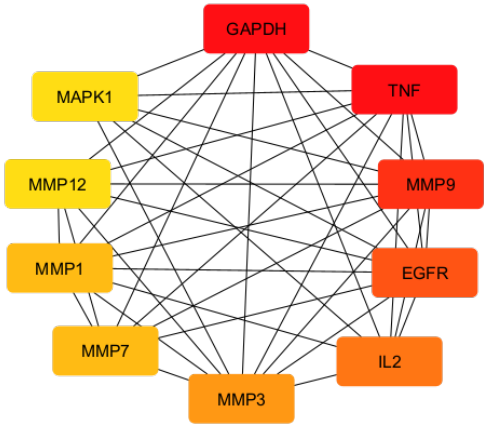

Figure 3. Top 10 hub targets of the PPI network: The method of Degree in cytoHubba was used to identify the top 10 PPI network connectivity hub targets. A red colour indicates a higher degree, and a yellow colour a lower degree.

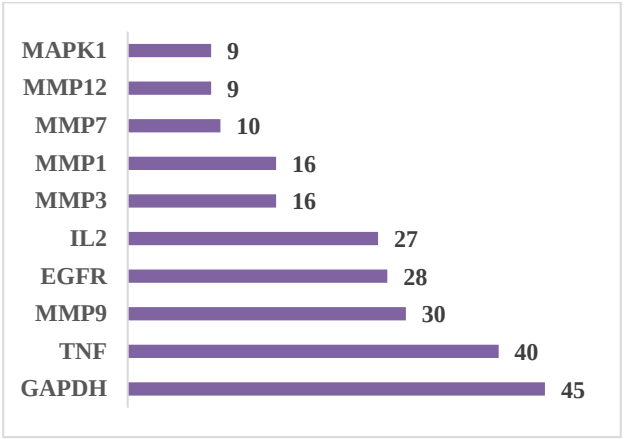

Figure 4. Bar Chart of Top 10 Hub Genes by Degree method with Scores.

GO and KEGG Pathway Enrichment Analysis

The online tool DAVID and Shiny GO were utilized to draw and describe the molecular mechanism by gene ontology enrichment and KEGG pathway analyses. The GO enrichment analysis consists of three major branches: Biological process, Molecular function, and Cellular component. According to the BP, these target genes mainly participate in Response to UV-A, Cellular response to UV-A, Cellular response to cadmium ion, Extracellular matrix organization, Extracellular to amyloid beta, response to light stimulus, Extracellular structure organization, External encapsulating structure organization, etc. According to the Cellular components, the target genes were significantly enriched in the GAIT complex, Multi-vesicular body internal vesicle, Ficolin-1-rich granule lumen, Ficolin-1-rich granule, Extracellular matrix, Extracellular space, Extracellular region and so forth.

The results obtained associated these central targets with Molecular Functions such as Collagen binding, Epidermal growth factor activated receptor activity, Epidermal growth factor binding, Interleukin-2-receptor binding, Opioid receptor, Metalloendopeptidase activity, Serine hydrolase activity, Nitric oxide synthase regulator activity, serine hydrolase activity, Phosphatase binding, Peptidase activity, Hydrolase activity and so forth.

Results from KEGG pathway enrichment analysis revealed that the predicted hub targets were related to pathways such as Bladder Cancer, IL-17 Signaling Pathway, Prostate Cancer, Melanoma, TNF Signaling Pathway, Estrogen Signaling Pathway, Endocrine resistance, Relaxin Signaling Pathway, Central carbon metabolism in cancer, HIF-1 Signaling Pathway, etc. Figure 5(A-D) displays a Bubble chart depicting the top enriched Gene Ontology terms.

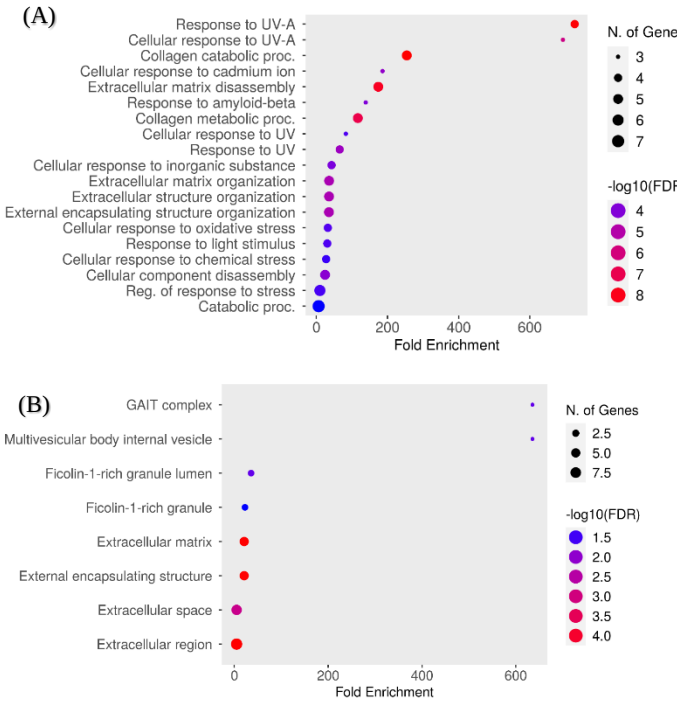

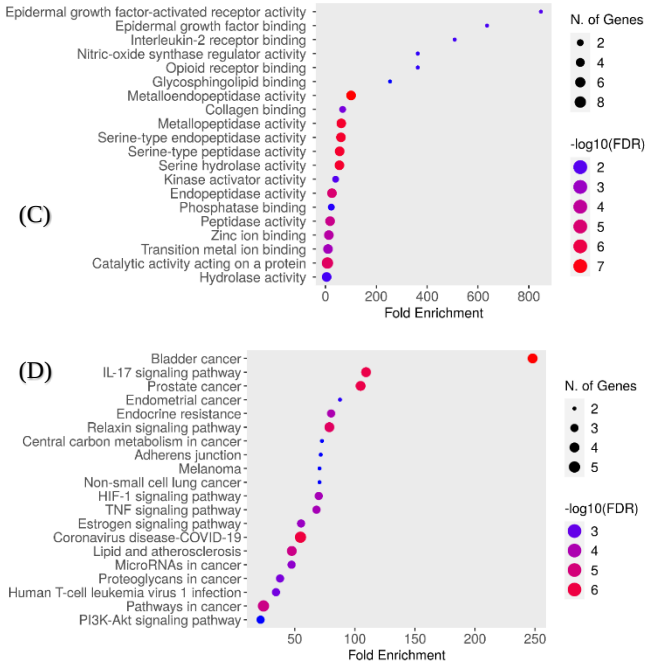

Figure 5. (A-D) depicts a bubble chart of the top enriched Gene Ontology terms (BP, CC, MF) and KEGG Pathways respectively.

The hierarchical clustering tree rearranges pathways with a large number of shared genes. The similarity between important pathways shown on the enrichment plot is, therefore, summarized. Larger dots correspond to more significant P-values. Figure 6 displays a hierarchical clustering tree illustrating the correlation among significant pathways identified in the enrichment analysis.

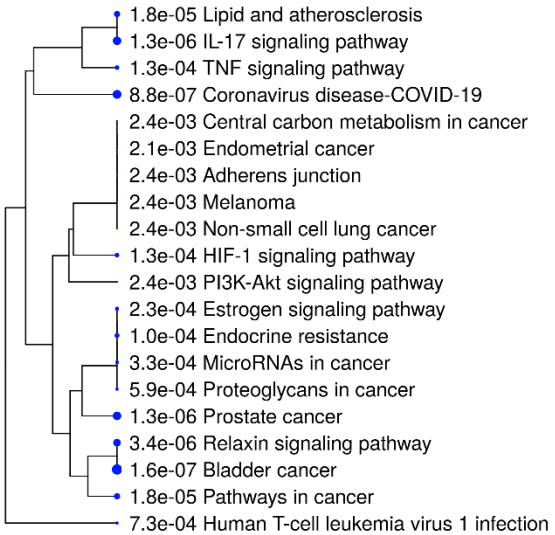

Figure 6. Hierarchical clustering tree – the correlation among significant pathways listed in the enrichment analysis.

Molecular Docking Analysis

Esculin has been used in identifying the top 10 Hub targets of bladder cancer, for which docking analysis was successful in

predicting the energy of their binding. Esculin has been utilized to identify the top 10 hub targets associated with bladder cancer, where docking analysis successfully predicted the binding energies of these targets. Among these, I focused on tumor necrosis factor (TNF) as a key hub target for docking studies. This selection is based on TNF's critical role in inflammation and cancer progression, providing a valuable opportunity to explore esculin's potential therapeutic effects in bladder cancer treatment. The results showed that TNF Hub Target (PDB ID: 1EXT) with Esculin had a score of −11.0 Kcal/mol, with Hydrogen interactions at the following amino acids: TYR B:106, ARG B:104, CYS B:96, GLU A:106, ASN A:110, THR B:93, ARG B:77, Hydrophobic interactions at the following amino acids: CYS B:96, ARG B:77, SER B:74. Table 1 shows Docking score of Esculin with TNF Hub Target. Figure 7 illustrates the 2-D docking conformations of Esculin with TNF Hub Target (PDB ID: 1EXT).

Table 1. Docking Score of Esculin with TNF Hub Target.

SL No	Hub Targets	PDB ID	Docking Score (Kcal/mol)	Hydrophobic Interactions	Hydrogen Bond Interactions
1	TNF	1EXT	-11.0	CYS B:96, ARG B:77, SER B:74.	TYR B:106, ARG B:104, CYS B:96, GLU A:106, ASN A:110, THR B:93, ARG B:77.

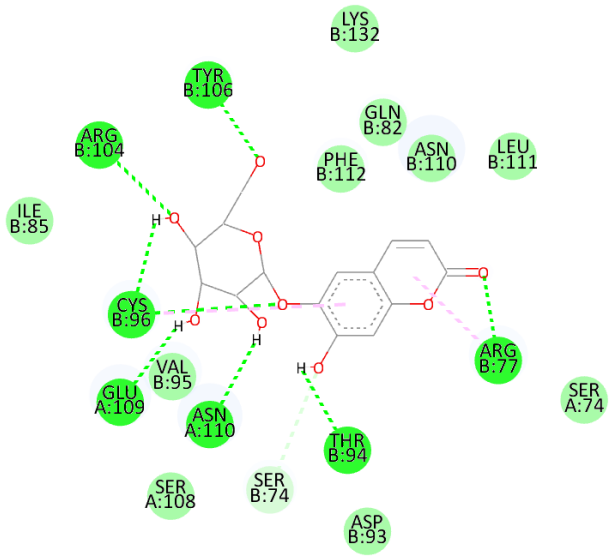

Figure 7. 2-D docking conformation of Esculin with TNF Hub Target (PDB ID: 1EXT).

ADMET Screening

The ADMET properties were evaluated using the online platforms SwissADME and ProToxIII. Figure 8 presents the 2D structures of Esculin. Various descriptors related to the ADMET profile were calculated and are detailed in Table 2 below.

Figure 8. 2D Structure of Esculin.

Table 2. Predicted Pharmacokinetics & ADMET parameters of Esculin predicted by SwissADME and ProTox 3.0 web server.

Parameters	Properties	Esculin
Drug-Likeness	Molecular Formula	$C_{15}H_{16}O_9$
	Molecular Weight (g/mol)	340.28
	Lipinski violations	0
	Ghose violations	1
	Veber violations	1
	Egan violations	1
	Muegge violations	0
Pharmacokinetic Parameters	Heavy atoms	24
	Aromatic heavy atoms	10
	Fraction Csp3	0.40
	Rotatable bonds (≤10)	3
	H-bond acceptors (≤10)	9
	H-bond donors (≤5)	5
	Molar Refractivity (40-130)	78.65
	TPSA (≤140Å^2)	149.82
	PAINS	0
	BRENKS	1
	LogP	1.33
Absorption	Pgp-substrate	No
	Bioavailability score	0.55
	GI absorption	Low
	Skin Permeation (Log Kp in cm/s)	-8.881
Distribution	Blood Brain Barrier	No
Metabolism	CYP1A2 inhibitor	No
	CYP2C19 inhibitor	No
	CYP2C9 inhibitor	No
	CYP2D6 inhibitor	No
	CYP3A4 inhibitor	No
Toxicity	Toxicity Class	5
	LD50	4000 mg/Kg
	Hepatotoxicity	No

Molecular Dynamics Simulation

A 50 ns Molecular Dynamics Simulation was carried out to study the stabilization of the protein-ligand complex and to get to know the ability of the Esculin as TNF Hub Protein, i.e. (PDB ID:1EXT). The results of the simulation were analysed by means of RMSD, RMSF, SASA, and hydrogen bonds. A triclinic box, solvated with TIP3P waters was used by 1EXT-Esculin Complex in the 50 ns simulation. Adding 49 Na^+ and 51 Cl^- ions neutralized the total charge of the system. The total system includes 79856 atoms. Computation of the RMSD of the protein backbone was done to ascertain that the structural stability of the system is maintained along the simulation. In Figure 12, it is observed that after an initial equilibration, RMSD values remain almost constant, which consequently means that the protein

structure had reached a stable conformation. The average RMSD over the last 50 ns of the simulation was 1.5 Å with a standard deviation of 0.2 Å. It suggests that the protein maintained its overall structure with very minimal deviation. RMSF analysis was carried out to study the flexibility of different regions within the protein. The RMSF plot Figure 13 underlines that lowest fluctuations were observed in the protein. On average, the RMSF of all residues was 1.2 Å, which reflects very low flexibility for most regions of the protein. To further understand the structure's stability, hydrogen bond interactions between the protein-ligand and protein-protein interactions were computed. The number of hydrogen bonds during the 50 ns of the simulation was found to be 1 to 6, huge fluctuations were observed during the equilibration phase of the simulations. The graph shown in Figure 14, shows that the protein maintained a stable network of hydrogen bonds throughout the simulation run. To get insight into the extent of exposure of the protein surface to the solvent, the SASA was estimated. Figure 15 shows the SASA values along the simulation time. The average SASA was 179.61 nm², with fluctuations attributed to conformational changes and interactions with the solvent. This would mean that although there were variations in this average surface exposure, there were increases in the accessibility of specific regions with this protein to the solvent.

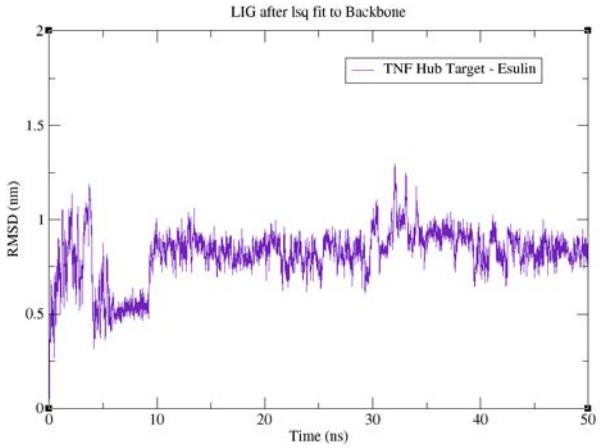

Figure 12. Root Mean Square Deviation (RMSD) of TNF Hub Target Protein (PDB ID:1EXT) with Esculin.

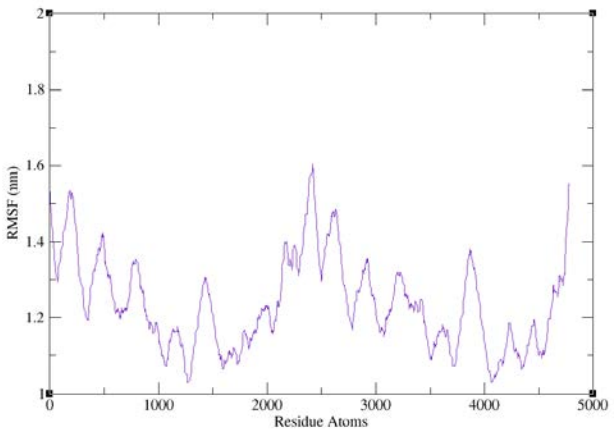

Figure 13. Root Mean Square Fluctuation (RMSF) of TNF Hub Target Protein (PDB ID:1EXT) with Esculin.

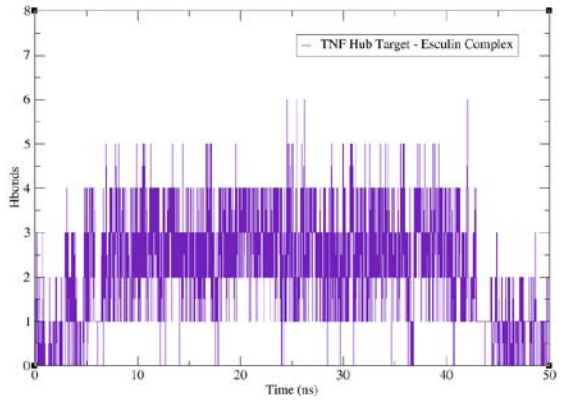

Figure 14. Number of Hydrogen bonds of TNF Hub Target Protein (PDB ID:1EXT) with Esculin.

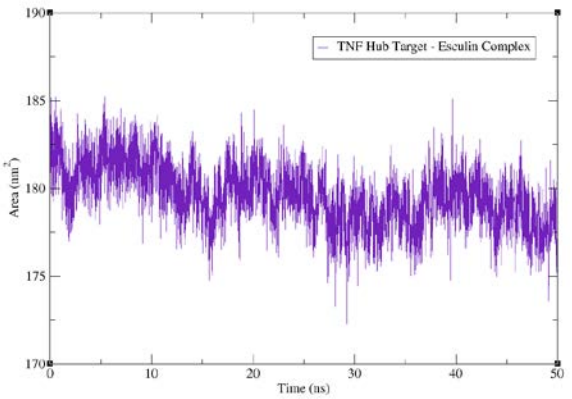

Figure 15. Solvent Accessible Surface Area (SASA) of TNF Hub Target (PDB ID:1EXT) with Esculin.

3.7 Molecular Mechanics Poison Boltzmann Surface Area (MM/PBSA)

The binding free energy calculations for the TNF hub target-Esculin complex were conducted using the Molecular Mechanics Poisson-Boltzmann Surface Area (MMPBSA) method to evaluate their affinities. The results indicated that TNF hub target-Esculin complex exhibited a favourable total binding free energy of -8.92 kcal/mol, suggesting a strong interaction with the TNF Hub Target protein. This favourable binding was largely attributed to significant contributions from van der Waals interactions (-16.1 kcal/mol) and electrostatic interactions (-3.57 kcal/mol), complemented by positive solvation effects, including a polar solvation energy (EPB) of 12.46 kcal/mol and a nonpolar solvation energy (ENPOLAR) of -1.71 kcal/mol, resulting in a Gibbs free energy of solvation (GGAS) of -19.67 kcal/mol and a total solvation energy (GSOLV) of 10.75 kcal/mol. The energy decomposition analysis revealed that specific residues in the binding pocket played crucial roles in stabilizing the TNF Hub Target – Esculin complex, underscoring its potential as a promising candidate for further exploration in drug development. Overall, these MMPBSA results, summarized in Table 3 align with findings from the MD simulations, highlighting the superior binding characteristics of TNF Hub Target – Esculin complex.

Table 3. Binding Free Energy Analysis of TNF Hub target-Esculin Complex Using MMPBSA Method.

Complex	VDwaals (Kcal/mol)	EEL (Kcal/mol)	EPB (Kcal/mol)	ENPOLAR (Kcal/mol)	GGAS (Kcal/mol)	GSOLV (Kcal/mol)	Total (Kcal/mol)
TNF Hub Target – Esculin complex	-16.1	-3.57	12.46	-1.71	-19.67	10.75	-8.92

3.8 Principal Component Analysis (PCA)

An investigation into principal component analysis (PCA) was carried out to explore the dynamic behaviour of key enzyme residues in the presence of ligands. The first three eigenvectors were selected for PCA analysis to assess the coordinated motion of all systems over the 50 ns simulation trajectory. The diagonalization of the covariance matrix of atomic fluctuations revealed eigenvalues of 612.02 nm² for the TNF Hub Target – Esculin complex (indigo) see Figure 16. The initial two principal components (PC1 and PC2) were utilized to create a 2D projection of the trajectory plots, highlighting the dynamic behaviour of the complex. In Figure 17, the projections of the two eigenvectors are displayed: TNF Hub Target – Esculin complex (indigo). The size of the clusters indicates the stability of the protein-ligand complex, where smaller clusters suggest greater stability and larger clusters indicate less stability. The trajectory plot showed that the TNF Hub Target – Esculin complex occupies a relatively smaller space, indicating higher stability.

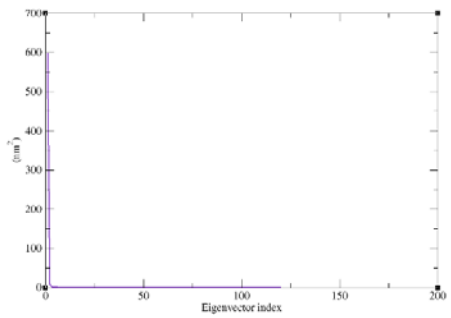

Figure 16. PCA plot of TNF Hub Target – Esculin complex (indigo).

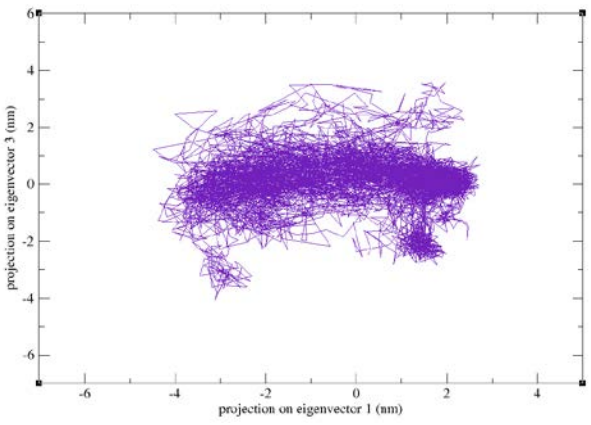

Figure 17. 2D projection of trajectories on eigenvectors showed different projections of TNF Hub Target – Esculin complex (indigo).

CONCLUSION

Network pharmacology combined with molecular docking studies was utilized to explore the role of Esculin in treating bladder cancer. This study employed these techniques to investigate the mechanisms of Esculin and its interactions with target proteins associated with bladder cancer. Based on KEGG pathways, a comprehensive analysis revealed multiple signalling pathways relevant to Esculin's therapeutic effects, including central carbon metabolism in cancer, TNF signalling, estrogen signalling, prostate cancer, melanoma, IL-17 signalling, endocrine resistance, and the HIF-1 signalling pathway. The 50 ns molecular dynamics simulations of the TNF-Esculin complex (PDB ID: 1EXT) demonstrated that both proteins maintained structural stability with minimal deviations. Analyses of RMSD, RMSF, hydrogen bond interactions, and SASA confirmed that the proteins achieved stable conformations. Binding free energy calculations using the Molecular Mechanics Poisson-Boltzmann Surface Area (MMPBSA) method further clarified the interaction dynamics, showing that the TNF-Esculin complex had a favourable total binding free energy of -8.92 kcal/mol. This interaction was primarily driven by van der Waals forces (-16.1 kcal/mol) and electrostatic interactions (-3.57 kcal/mol), along with significant solvation effects, indicating a strong binding mechanism. Energy decomposition analysis highlighted specific residues within the binding pocket that are crucial for stabilizing the complex, underscoring Esculin's potential for drug development. Principal component analysis (PCA) of the molecular dynamics simulations illustrated the dynamic behaviour of the TNF-Esculin complex, with the first three eigenvectors showing coordinated motion and a high degree of stability, as indicated by reduced spatial occupation in trajectory plots. Overall, these findings, including MMPBSA results and PCA analysis, provide strong support for further investigation of Esculin as a novel therapeutic agent for bladder cancer, necessitating additional experimental validation and drug development efforts. This work lays a foundation for future studies in drug discovery and development, aiming for more effective and targeted treatments. Research in medication development can benefit from these insights to create more specific and effective therapies.

CONFLICT OF INTEREST STATEMENT

Author do not have any academic or financial interest that might have influenced this study.

ETHICAL DECLARATIONS

Animal studies not included.

CLINICAL TRIAL INFORMATION

Clinical studies not involved in this study.

REFERENCES AND NOTES

1. B.S. Chhikara, K. Parang. Global Cancer Statistics 2022: the trends projection analysis. *Chem. Biol. Lett.* **2023**, 10 (1), 451.
2. K.E. Andersson, A. Arner. Urinary bladder contraction and relaxation: Physiology and pathophysiology. *Physiol. Rev.* **2004**, 84 (3), 935–986.

3. J. Mushtaq, R. Thurairaja, R. Nair. Bladder cancer. *Surg.* **2019**, 37 (9), 529–537.
4. V. Lumb, P. Karwal. Intravesical BCG immunotherapy for Non-Muscle Invasive Bladder Cancer during COVID-19 pandemic: Mutual impact and implications. *Chem. Biol. Lett.* **2022**, 9 (2), 267.
5. N.D. Freedman, D.T. Silverman, A.R. Hollenbeck, A. Schatzkin, C.C. Abnet. Association between smoking and risk of bladder cancer among men and women. *Jama* **2011**, 306 (7), 737–745.
6. B. Turner, L. Drudge-Coates. Bladder cancer: risk factors, diagnosis and treatment. *Cancer Nurs. Pract.* **2012**, 11 (7), 30–37.
7. A. Owczarek, J. Kolodziejczyk-czepas, J. Woźniak-serwata, et al. Potential activity mechanisms of aesculus hippocastanum bark: Antioxidant effects in chemical and biological in vitro models. *Antioxidants* **2021**, 10 (7), 995.
8. S.K. Wang, T.X. Chen, W. Wang, et al. Aesculetin exhibited anti-inflammatory activities through inhibiting NF-κB and MAPKs pathway in vitro and in vivo. *J. Ethnopharmacol.* **2022**, 296, 115489.
9. M.M. Lay, S.A. Karsani, S. Mohajer, S.N. Abd Malek. Phytochemical constituents, nutritional values, phenolics, flavonols, flavonoids, antioxidant and cytotoxicity studies on Phaleria macrocarpa (Scheff.) Boerl fruits. *BMC Complement. Altern. Med.* **2014**, 14 (1), 152.
10. A. Owczarek, J. Kołodziejczyk-Czepas, P. Marczuk, et al. Bioactivity potential of aesculus hippocastanum l. Flower: Phytochemical profile, antiradical capacity and protective effects on human plasma components under oxidative/nitrative stress in vitro. *Pharmaceuticals* **2021**, 14 (12), 1301.
11. S. Anand, A. Chaudhuri, N. Chopra, et al. A Comprehensive Review of Therapeutical and Ethnobotanical Aspects, Phytoconstituent and Pharmacological Activity of Aesculus indica. *Pharmacognosy Res.* **2024**, 16 (2), 203–210.
12. A.L. Hopkins. Network pharmacology: The next paradigm in drug discovery. *Nat. Chem. Biol.* **2008**, 4 (11), 682–690.
13. M. Yousef, J. ALLMER. Deep learning in bioinformatics. *Turkish J. Biol.* **2023**, 47 (6), 366–382.
14. M. Kanehisa. The KEGG Database. In *Novartis Foundation Symposium*; John Wiley & Sons, Ltd, Chichester, UK, **2002**; Vol. 247, pp 91–103.
15. J.K.X. Maier, P. Labute. Assessment of fully automated antibody homology modeling protocols in molecular operating environment. *Proteins Struct. Funct. Bioinforma.* **2014**, 82 (8), 1599–1610.
16. S. Kim, J. Chen, T. Cheng, et al. PubChem 2023 update. *Nucleic Acids Res.* **2023**, 51 (D1), D1373–D1380.
17. D. Gfeller, A. Grosdidier, M. Wirth, et al. SwissTargetPrediction: a web server for target prediction of bioactive small molecules. *Nucleic Acids Res.* **2014**, 42 (W1), W32–W38.
18. M. Kuhn, C. von Mering, M. Campillos, L.J. Jensen, P. Bork. STITCH: Interaction networks of chemicals and proteins. *Nucleic Acids Res.* **2008**, 36 (SUPPL. 1), 684– 688.
19. G. Stelzer, N. Rosen, I. Plaschkes, et al. The GeneCards suite: From gene data mining to disease genome sequence analyses. *Curr. Protoc. Bioinforma.* **2016**, 2016, 1.30.1-1.30.33.
20. C. v. Mering. STRING: a database of predicted functional associations between proteins. *Nucleic Acids Res.* **2003**, 31 (1), 258–261.
21. R. Saito, M.E. Smoot, K. Ono, et al. A travel guide to Cytoscape plugins. *Nat. Methods* **2012**, 9 (11), 1069–1076.
22. C.-H. Chin, S.-H. Chen, H.-H. Wu, et al. cytoHubba: identifying hub objects and sub-networks from complex interactome. *BMC Syst. Biol.* **2014**, 8 (S4), S11.
23. P. Shannon, A. Markiel, O. Ozier, et al. Cytoscape: A Software Environment for Integrated Models of Biomolecular Interaction Networks. *Genome Res.* **2003**, 13 (11), 2498–2504.
24. B.T. Sherman, M. Hao, J. Qiu, et al. DAVID: a web server for functional enrichment analysis and functional annotation of gene lists (2021 update). *Nucleic Acids Res.* **2022**, 50 (W1), W216–W221.
25. G. Dennis, B.T. Sherman, D.A. Hosack, et al. DAVID: Database for Annotation, Visualization, and Integrated Discovery. *Genome Biol.* **2003**, 4 (9), 3.
26. S.X. Ge, D. Jung, D. Jung, R. Yao. ShinyGO: A graphical gene-set enrichment tool for animals and plants. *Bioinformatics*. Bioinformatics (Oxford, England 2020, pp 2628–2629.
27. M. Kanehisa, S. Goto. KEGG: Kyoto Encyclopedia of Genes and Genomes. *Nucleic Acids Res.* **2000**, 28 (1), 27–30.
28. E. Harder, W. Damm, J. Maple, et al. OPLS3: A Force Field Providing Broad Coverage of Drug-like Small Molecules and Proteins. *J. Chem. Theory Comput.* **2016**, 12 (1), 281–296.
29. G. Madhavi Sastry, M. Adzhigirey, T. Day, R. Annabhimoju, W. Sherman. Protein and ligand preparation: parameters, protocols, and influence on virtual screening enrichments. *J. Comput. Aided. Mol. Des.* **2013**, 27 (3), 221–234.
30. V. Rustagi, S.R.R. Gupta, A. Singh, I.K. Singh. Beyond trial and error: Leveraging advanced software for Therapeutic discovery. *Chem. Biol. Lett.* **2025**, 12 (1), 1251.
31. V.K. Maurya, S. Kumar, M. Singh, V. Saxena. Molecular docking and dynamic studies of novel phytoconstituents in an investigation of the potential inhibition of protein kinase C- beta II in diabetic neuropathy. *J. Mol. Chem.* **2023**, 3 (2), 589.
32. P. Banerjee, E. Kemmler, M. Dunkel, R. Preissner. ProTox 3.0: A webserver for the prediction of toxicity of chemicals. *Nucleic Acids Res.* **2024**, 52 (W1), W513–W520.
33. H.J.C. Berendsen, D. van der Spoel, R. van Drunen. GROMACS: A message-passing parallel molecular dynamics implementation. *Comput. Phys. Commun.* **1995**, 91 (1–3), 43–56.
34. I. Soteras Gutiérrez, F.Y. Lin, K. Vanommeslaeghe, et al. Parametrization of halogen bonds in the CHARMM general force field: Improved treatment of ligand–protein interactions. *Bioorganic Med. Chem.* **2016**, 24 (20), 4812–4825.
35. M. Bugnon, M. Goullieux, U.F. Röhrig, et al. SwissParam 2023: A Modern Web-Based Tool for Efficient Small Molecule Parametrization. *J. Chem. Inf. Model.* **2023**, 63 (21), 6469–6475.
36. K. Vanommeslaeghe, E. Hatcher, C. Acharya, et al. CHARMM general force field: A force field for drug-like molecules compatible with the CHARMM all-atom additive biological force fields. *J. Comput. Chem.* **2010**, 31 (4), 671–690.
37. A.F. Voter. A method for accelerating the molecular dynamics simulation of infrequent events. *J. Chem. Phys.* **1997**, 106 (11), 4665–4677.
38. B. Hess, H. Bekker, H.J.C. Berendsen, J.G.E.M. Fraaije. LINCS: A Linear Constraint Solver for molecular simulations. *J. Comput. Chem.* **1997**, 18 (12), 1463–1472.
39. X. Wang, S. Ramírez-Hinestrosa, J. Dobnikar, D. Frenkel. The Lennard-Jones potential: when (not) to use it. *Phys. Chem. Chem. Phys.* 22 (19), 10624–10633.
40. U. Essmann, L. Perera, M.L. Berkowitz, et al. A smooth particle mesh Ewald method. *J. Chem. Phys.* **1995**, 103 (19), 8577–8593.
41. M.S. Valdés-Tresanco, M.E. Valdés-Tresanco, P.A. Valiente, E. Moreno. Gmx_MMPBSA: A New Tool to Perform End-State Free Energy Calculations with GROMACS. *J. Chem. Theory Comput.* **2021**, 17 (10), 6281–6291.
42. C.B.C. Ikpa, N.N. Chidozie-Ikpa. Molecular docking of phytochemical compounds in Cucurbita maxima with anti-prostate cancer activity. *J. Mol. Chem.* **2024**, 4 (1), 685.